*Int. J. Electrochem. Sci.*, 12 **(2017)** 7365 – 7376, doi: 10.20964/2017.08.48

**International Journal of ELECTROCHEMICAL SCIENCE**
www.electrochemsci.org

# Growth of Worm-Like and Flower-Like Molybdenum Disulfide on Graphene Nanosheets for Sensitive Determination of Dopamine

*Guangran Ma, Hui Xu, Fugang Xu*[*]*, Li Wang*[*]

College of Chemistry and Chemical Engineering, Jiangxi Normal University, Nanchang 330022, People's Republic of China
[*]E-mail: xfg12315@hotmail.com (F.G. Xu); lwang@jxnu.edu.cn (L. Wang).

*Received:* 9 May 2017 / *Accepted:* 7 June 2017 / *Published:* 12 July 2017

In this article, a three dimensional hybrid named as 3D-f-$MoS_2$-rGO composed of worm-like and flower-like molybdenum disulfide ($MoS_2$) grown on reduced graphene oxide (rGO) was prepared for sensitive electrochemical detection of dopamine (DA). The hybrid 3D-f-$MoS_2$-rGO was prepared by a facile hydrothermal reaction, and its structure and composition were characterized by scanning electron microscopy (SEM), energy-dispersive X-ray spectrum (EDX) and Raman spectroscopy. The electrochemical behavior and electrocatalytic property of the 3D-f-$MoS_2$-rGO hybrid were explored by electrochemical impedance spectroscopy (EIS), cyclic voltammetry (CV) and differential pulse voltammetry (DPV). The results revealed that the 3D-f-$MoS_2$-rGO hybrid displayed much higher catalysis towards dopamine oxidation than that of single component rGO or $MoS_2$ due to the synergistic interaction between rGO and $MoS_2$. The hybrid modified electrode was used for non-enzymatic detection of dopamine, which showed a linear response range of 0.2 μM to 150 μM, a detection limit of 0.05 μM, a good selectivity and reproducibility. Furthermore, the sensor also displayed satisfactory results in real samples analysis, which demonstrates its great potential in practical applications.

**Keywords:** molybdenum disulfide, graphene, dopamine, electrochemical sensor, hybrid material

## 1. INTRODUCTION

As a graphene analogue, molybdenum disulfide ($MoS_2$) nanosheet, a 2D transition metal dichalcogenides with Mo layer sandwiched between two sulfur layers by covalent forces, has attracted increasing interest nowadays due to their excellent optical, mechanical, electronic and catalytic properties [1,2] and their promising applications in lithium ion batteries, transistors and catalytic

hydrogen evolution reaction (HER) [3,4]. Compared to these applications, less attentions have been put into its application for electrochemical sensor, which might be ascribed to two factors. On the one hand, the conductivity of $MoS_2$ is much lower than graphene or other carbon nanomaterials, and thus more electrochemical sensors are fabricated based on carbon nanomaterials [5]. On the other hand, the aggregation of two dimensional $MoS_2$ sheets will not only greatly reduce the surface area, but also bury lots of active edge sites inside, which cannot react with analytes [6]. These issues restrict the further application of $MoS_2$ in electrochemical sensing. Therefore, it is urgent to develop a new approach to further explore and accelerate the application of $MoS_2$ in electrochemical sensors.

At present, integrating $MoS_2$ with other functional nanomaterials such as noble metal particles [7-9], conducting polymers [10], or carbon nanomaterials [11,12] are widely used to improve the performance of $MoS_2$ based electrochemical devices. For example, Au NPs, Pt NPs [7], gold nanorods [8] or Au-Pd nanoparticles [9] were used to decorate $MoS_2$ to construct sensitive electrochemical sensors. However, the introduction of noble metal particles may increase the cost of the sensors, and the catalysis mainly comes from the noble metal particles while $MoS_2$ usually acts as a supporting matrix, whose catalysis is not obviously shown. In addition to noble metal nanoparticles, graphene is also widely used to prepare $MoS_2$ based composite due to its large specific surface area, high electrical conductivity, easy processing, and low cost of preparation. For example, graphene supported $MoS_2$ sheet was used for cysteamine [13] or folic acid [14] detection. Nevertheless, most of these composites of graphene with $MoS_2$ still show two dimensional morphology and suffer from aggregation.

Besides developing $MoS_2$ based composite or hybrid, controlling the structure or morphology of $MoS_2$ is another efficient approach to tune the performance of $MoS_2$ based devices. Zhou et al. used salt template to prepare a 3D honey-comb like $MoS_2$ for lithium-ion battery anode [15]; Zhai et al. prepared flower-like $MoS_2$ for glucose detection [16]; Shuai et al. prepared $MoS_2$ microcubes as platform for microRNA-21 detection [17]. Although the active site and surface area of these $MoS_2$ are guaranteed, the conductivity of these $MoS_2$ nanomaterials are still relative low. Thus, a new $MoS_2$ hybrid should be prepared for sensitive electrochemical sensors.

In this study, a three-dimensional (3D) hybrid 3D-f-$MoS_2$-rGO composed of work-like and flower-like $MoS_2$ grown on graphene sheet was prepared and its performance for the sensitive detection of dopamine (DA) was investigated. The 3D-f-$MoS_2$-rGO hybrid can be obtained by simple hydrothermal treatment of $MoS_2$ precursors and GO sheets. SEM, EDS, Raman spectroscopy and electrochemical methods were used to characterize the structure and electrochemical properties of the 3D f-$MoS_2$-rGO. The introduction of graphene could elevate the conductivity of $MoS_2$ based hybrid and the 3D flower-like $MoS_2$ greatly reduce the aggregation of the graphene sheet. Due to these synergistic interaction, the 3D-f-$MoS_2$-rGO hybrid showed much higher electrocatalytic activity than that of single component $MoS_2$ or rGO for DA oxidation. A non-enzymatic sensor based on 3D-f-$MoS_2$-rGO showed a wide linear range of 0.2 μM to 150 μM and a low detection limit of 0.05 μM for dopamine detection. In addition, the sensor also exhibited good selectivity and acceptable reproducibility, and can be used for DA sensing in real samples.

## 2. EXPERIMENTAL METHODS

### *2.1. Chemicals and solutions*

Graphite (325mesh), dopamine (DA), ascorbic acid (AA) and uric acid (UA) were purchased from Alfa Aesar. Nafion and potassium chloride (KCl) were obtained from Sigma-Aldrich. $MoO_3$ (99.9% purity), KSCN (98.5% purity) and phosphate salt ($NaH_2PO_4$ and $Na_2HPO_4$) were purchased from Shanghai Sinopharm Chemical Reagent Co. Ltd. (Shanghai, China). All reagents were of analytical grade and used without further purification. Phosphate buffer solutions (PBS) with pH = 7.0 was used as the supporting electrolyte in this study. Ultrapure water (≥18.2 MΩ) produced by Millipore system was used for the preparation of buffer solutions.

### *2.2. Preparation of GO, rGO, $MoS_2$, and 3D-f-$MoS_2$-rGO*

#### *2.2.1. Preparation of graphene oxide*

Graphene oxide (GO) was prepared according to a modified Hummer's method involving the steps of graphite oxidation and subsequent exfoliation [18].

#### *2.2.2. Preparation of 3D-f-$MoS_2$-rGO hybrid*

To grow worm-like and flower-like $MoS_2$ on graphene, a facile hydrothermal approach was developed. Briefly, 0.0135 g $MoO_3$ powder and 0.0228 g KSCN were added into GO suspension (2 mg/mL) in a mixed solvent of 2.5 mL distilled water and 2.5 mL ethanol. The mixture was intensively ultrasonicated for 30 min to form a uniform suspension. Then the solution was sealed in a Teflon-lined autoclave and maintained at 200℃ for 16 h. After the autoclave cooled down to the room temperature, the black hydrogel was fully immersed in water to exchange the ethanol absorbed inside the hydrogel. This step was then repeated several times, and finally 3D-f-$MoS_2$-rGO was obtained after freeze-drying the hydrogel for 12 h.

#### *2.2.3. Synthesis of $MoS_2$ and rGO*

For comparison, single component $MoS_2$ or rGO was also prepared in a procedure similar to that of 3D-f-$MoS_2$-rGO, except that no GO sheet or no $MoS_2$ precursor was added, respectively.

### *2.3. Electrochemical measurements*

Electrochemical measurements were carried out with a computer-controlled CHI 750 D electrochemical workstation to study the electrochemical activities of the prepared materials. All the electrochemical measurements were carried out in a conventional three-electrode system: containing a platinum wire as the auxiliary electrode, a Ag/AgCl (in 3 M KCl, aq.) as the reference electrode, and

single component $MoS_2$, rGO or the hybrid 3D-f-$MoS_2$-rGO modified glassy carbon electrodes (GCE) as the working electrode. Freshly prepared phosphate buffer solution (pH 7.0) was used as the supporting electrolyte. Cyclic voltammetry (CV) and differential pulse voltammetry (DPV) were carried out in 0.1 M PBS (pH =7.0) in the range of -0.2 V to 0.6 V. Electrochemical impedance spectroscopy (EIS) measurements were conducted with 5 mV amplitude in the frequency range of 0.1 Hz to 100 kHz at the open circuit potential.

For typical construction of the 3D-f-$MoS_2$-rGO modified electrode, 2.0 mg of the 3D-f-$MoS_2$-rGO hybrid was dispersed into 2.0 mL water under ultrasonication to form a homogeneous suspension. Next, 5 μL of the suspension was cast on the clean GCE and dried naturally, followed by casting a layer of 5 μL Nafion (0.05 wt%) to fix the deposit on the electrode surface. Thus modified electrode was denoted as 3D-f-$MoS_2$-rGO/GCE. For comparison, single component material $MoS_2$ or rGO was also used to modify GCE, and the modified electrodes were denoted as $MoS_2$/GCE and rGO/GCE, respectively.

### *2.4 Characterization*

Scanning electron microscopy (SEM) images were captured using an S-3400 (Hitachi, Japan) SEM equipped with an energy-dispersive X-ray (EDX) analyzer. Raman spectra were acquired on a LABRAM-HR Raman system (Horiba, Jobin-Yvon, France) with a 633 nm He-Ne laser.

## 3. RESULTS AND DISCUSSION

### *3.1. Morphologies and structure characteristics of 3D $MoS_2$/rGO*

To data, $MoS_2$ with various micro/nano-structures have been prepared by different approaches [19-21]. Here, a facile hydrothermal approach was developed to prepare 3D worm-like and flower-like MoS2 anchored on graphene sheet scaffold. The morphologies and microstructures of 3D-f-MoS2-rGO hybrid were investigated using SEM.

As shown in Fig. 1a, sheet-like products are vertically, slantwise, or parallelly piled on the substrate forming a 3D porous structure. It seems that these sheets have rough surface. Close view in Fig. 1b reveals worm-like $MoS_2$ ridge (200 nm in length) and flower-like $MoS_2$ (300-600 nm in diameter) are well formed on the rGO sheets. Besides these, some large protrusion structure can also be observed. It seems the protrusion is the intermediate stage between the worm-like and flower-like product. These structures indicate the growth process of $MoS_2$ on graphene may be as following: $MoS_2$ first nuclear on graphene, and then grow into worm-like $MoS_2$ in the early stage, and then $MoS_2$ ridge continuous to grow into $MoS_2$ sheets, which protrude from the rGO surface. Many $MoS_2$ sheet interlace with each other and thus flower-like $MoS_2$ on rGO sheets are formed. Further magnified image in Fig. 1c shows these $MoS_2$ flowers are composed of cross-liked $MoS_2$ nanosheets, which is consistent to our hypothesis of the growth process of $MoS_2$. Moreover, the flower-like $MoS_2$ are closely anchored on the rGO sheet scaffold. This close contact between $MoS_2$ and graphene may facilitate the electron transfer, which is beneficial to improve the performance of corresponding sensor.

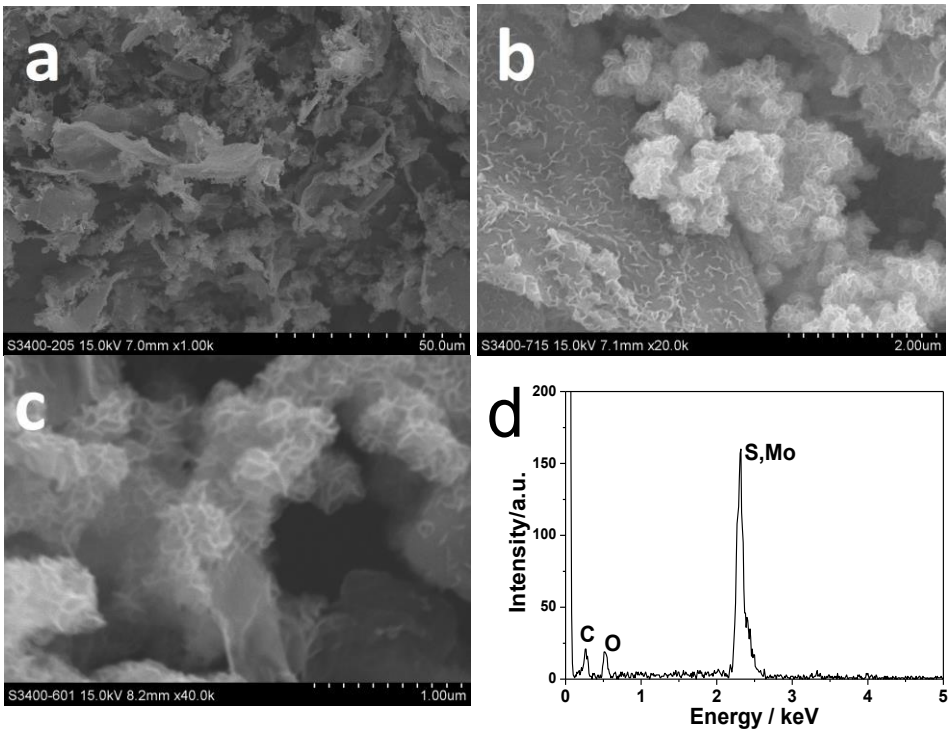


**Figure 1.** (a-c) SEM images of 3D-f-$MoS_2$-rGO hybrid, and (d) EDS results of 3D-f-$MoS_2$-rGO hybrid.

The EDS result reveals that the product is mainly composed of element C, O from GO, and Mo, S from $MoS_2$. These results from SEM and EDS confirmed the successful preparation of 3D-f-$MoS_2$-rGO hybrid. It is noticeable that flower-like $MoS_2$ could also be produced without introducing GO sheet, but those products display a serious aggregation, which implies many active sites may be buried inside. Therefore, the interaction between GO and $MoS_2$ could improve the dispersity of the hybrid, and thus increase the active surface area, expose more active sites, which are helpful for improving the performance of a sensor.

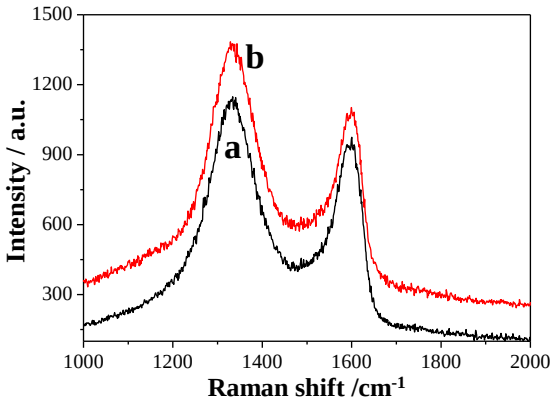


**Figure 2.** Raman spectrum of rGO (a) and 3D-f-$MoS_2$-rGO hybrid (b).

Fig. 2 shows the Raman spectra of rGO (curve a) and 3D-f-$MoS_2$-rGO hybrid (curve b). The Raman spectrum of rGO shows characteristic D and G bands at 1334 and 1599 $cm^{-1}$ [22], respectively. After growing worm-like and flower-like $MoS_2$ on it, the Raman spectrum displays a similar pattern, but with an increase in the intensity ratio of D band to G band ($I_D/I_G$ = 1.26 for 3D-f-$MoS_2$-rGO versus $I_D/I_G$ = 1.14 for rGO). The increased intensity ratio suggests a strong interaction between $MoS_2$ and rGO scaffold [23], which is good to enhance the electron transfer.

### *3.2. Electrochemical impedance spectroscopy characterization*

One of the aim to integrate graphene with $MoS_2$ is to overcome the shortage of relative low conductivity of $MoS_2$. To confirm the effect of graphene on the conductivity of the hybrid material, electrochemical impedance spectroscopy (EIS) was used to investigate the electrochemical impedance changes of different materials modified electrodes.

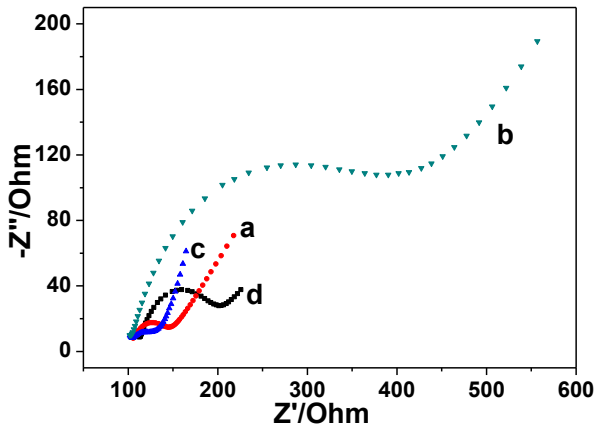


**Figure 3.** Electrochemical impedance spectroscopy of bare GCE (a), $MoS_2$/GCE (b), rGO/GCE (c), and 3D-f-$MoS_2$-rGO/GCE (d) in 5 mM $Fe(CN)_6^{3-/4-}$ containing 0.1 M KCl solution.

As can be seen in Fig. 3, EIS curve of bare GCE (curve a) shows a semi-circle pattern with small diameter, indicating a low electron transfer resistance. After $MoS_2$ was coated onto GCE, the EIS curve (curve b) still shows a similar semi-circle pattern but with much larger diameter, implying the coated $MoS_2$ obviously increases the electron transfer resistance due to its low conductivity. If rGO was used to modify GCE, the diameter of EIS curve (curve c) is even smaller than that of bare GCE, demonstrating rGO could improve the electron transfer due to its high conductivity. For the hybrid modified electrode 3D-f-$MoS_2$-rGO/GCE, EIS curve (curve d) also display a semicircle pattern, but the diameter is much smaller than that of $MoS_2$/GCE, and only a little larger than that of bare GCE or rGO/GCE. These EIS results confirm that the introduction of rGO could obviously improve the conductivity of the hybrid, and thus enhance the electron transfer efficiency at sensing interface.

*3.3. Electrocatalytic behaviors of modified electrodes*

The unique morphology, good conductivity and synergistic interaction between $MoS_2$ and rGO imply that the hybrid may have great potential in catalysis and electrochemical sensing. Here, the 3D-f-$MoS_2$-rGO hybrid was used to modify GCE and its electrocatalysis towards dopamine oxidation was investigated.

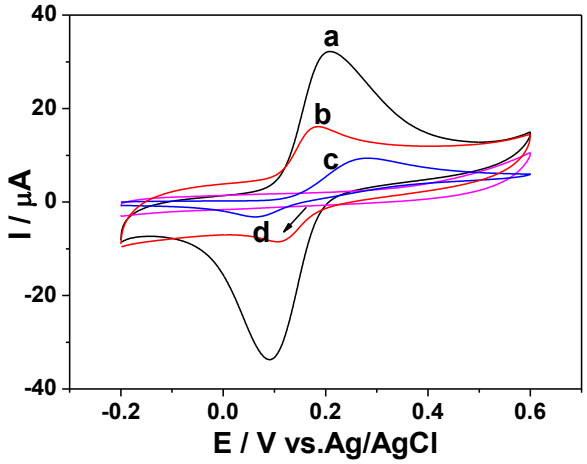


**Figure 4.** CVs obtained at (a) 3D-f-$MoS_2$-rGO/GCE, (b) rGO/GCE and (c) $MoS_2$/GCE in 0.1 M phosphate buffer (pH = 7) containing 1 mM DA at the scan rate of 50 mV $s^{-1}$. (d) CV of 3D-f-$MoS_2$-rGO/GCE in 0.1 M phosphate buffer (pH 7) in absence of DA.

Fig. 4 displays the cyclic voltammograms (CVs) of different material modified electrodes in 0.1 M PBS (pH 7.0) in the absence or presence of dopamine. In the absence of dopamine, the 3D-f-$MoS_2$-rGO/GCE (curve d) does not show obvious redox response. After dopamine is added into the electrolyte, the quasi-reversible redox peaks of dopamine are observed on all the modified electrodes [24], but with different redox peak potentials and redox current responses. The $MoS_2$/GCE (curve c) displays the highest redox over-potential of dopamine, which shows an anodic peak at 0.3 V and a cathodic peak at about 0.04V. The large peak potential difference ($\Delta Ep = Epa - Epc$= 0.26 V) can be ascribed to the low conductivity of $MoS_2$, which has been confirmed by EIS result. For rGO/GCE (curve c), an anodic peak at 0.18 V, and a cathodic peak at 0.11 V are observed. *$\Delta Ep$ is reduced to 0.07 V*, which is greatly reduced compared to that of $MoS_2$/GCE (curve b). This can be ascribed to the good conductivity of rGO, which facilitates the electron transfer at the modified electrode interface. For 3D-f-$MoS_2$-rGO/GCE (curve a), the $\Delta Ep$ is 0.11 V, which is slightly increases compared to that of rGO/GCE, but still obviously lower than that obtained on $MoS_2$/GCE. Importantly, the redox current of dopamine on 3D-f-$MoS_2$-rGO/GCE is much large than those obtained on rGO/GCE and $MoS_2$/GCE. The low oxidation current and high catalytic current indicates that 3D-f-$MoS_2$-rGO/GCE display much higher catalysis towards the oxidation of dopamine than single component rGO or $MoS_2$. This enhanced catalysis of 3D-f-$MoS_2$-rGO/GCE can be ascribed to the synergistic interaction between rGO and $MoS_2$: on the one hand, rGO sheet with high conductivity could accelerate the electron

transfer, thus the *ΔEp* decreases and redox current increases; on the other hand, $MoS_2$ and rGO form a 3D worm-like and flower-like structures in the hybrid, thus the aggregation of rGO or $MoS_2$ sheet in single component product is greatly reduced. As a consequence, more active surface is exposed to take part in the catalytic reaction, leading to a higher current response. In a word, synergistic effects between $MoS_2$ and rGO endow the hybrid a good catalysis to achieve the oxidation of DA at a relatively low potential with high oxidation current.

The electrochemical behavior of 3D-f-$MoS_2$-rGO/GCE for dopamine oxidation was also investigated by CV at different scan rates.

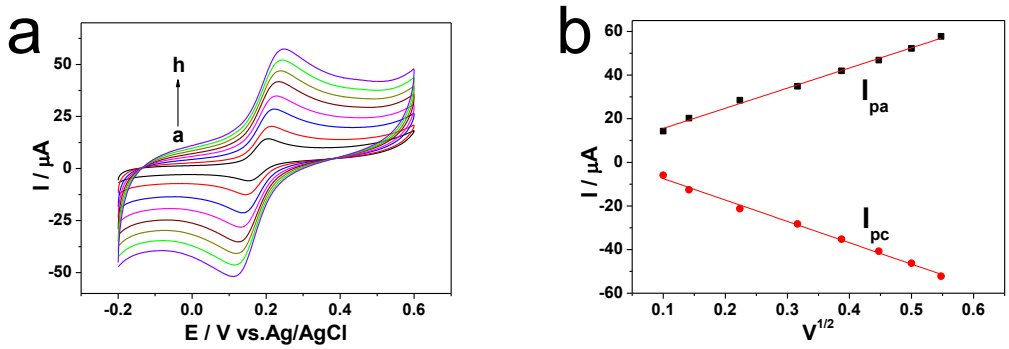


**Figure 5.** CVs of 3D-f-$MoS_2$-rGO/GCE in phosphate buffer (pH 7) containing 1 mM DA at different scan rates (a to h: 10 to 300 mV $s^{-1}$). Inset: Plot of $I_{pa}$ and $I_{pc}$ versus $v^{1/2}$.

The results in Fig. 5a clearly show that both the anodic and cathodic peak currents of dopamine increase with increasing the scan rate from 10 mV/s to 300 mV/s. The redox peak currents of DA display a linear increase with the square root of the scan rates, and the regression equations can be described as $I_{pa}$ = 92.3802 $v^{1/2}$ + 6.3117, $R^2$ = 0.9954 and $I_{pc}$ = -98.0183 $v^{1/2}$ + 2.3316, $R^2$ = 0.9950, respectively. This reveals that the oxidation of DA at 3D-f-$MoS_2$-rGO/GCE is a diffusion controlled process [25].

### *3.5. Determination of DA by DPV*

The unique structure, high conductivity, good catalysis of 3D-f-$MoS_2$-rGO/GCE imply that the hybrid can be used for dopamine detection. Since DPV usually has high sensitivity than CV, so DPV was used for dopamine detection.

Fig. 6 presents the DPV curves obtained on 3D-f-$MoS_2$-rGO/GCE in the presence of various concentrations of DA in PBS buffer. As shown in Fig. 6a, the oxidation peak current of DA steadily increases as more dopamine is added. The calibration curve reveals that the oxidation peak current linearly increases with concentration of dopamine from 0.2 μM to 150 μM (Fig. 6b), and the linear regression equation is $I$ (μA) = 0.2270 $c$ (μM) + 0.5360 with a correlation coefficient of $R^2$ = 0.9876. The detection limit is estimated to be 0.05 μM based on the signal-to-noise ratio of 3. It is observed that the detection limit and linear range of this 3D-f-$MoS_2$-rGO based sensor is superior to many previously reported DA sensors, such as Pd-rGO/GCE [26], Au NP-PANI/GCE [29], and GR/GCE

[34], which are listed in Table 1, confirming that the hybrid may have great potential in catalysis and electrochemical sensing.

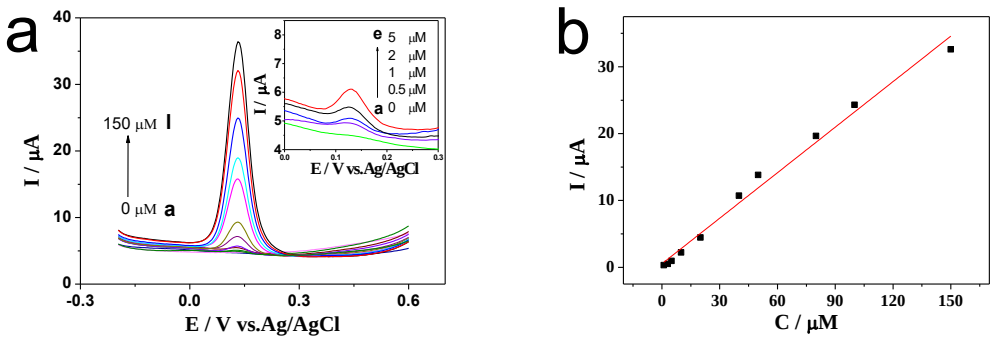


**Figure 6.** DPV of 3D-f-$MoS_2$-rGO/GCE in 0.1 M PBS (pH 7) with different concentrations of DA (from a to l: 0, 0.5, 1, 2, 5, 10, 20, 40, 50, 80, 100 and150 μM). $R^2$ = 0.9876.

**Table 1.** Comparison of different modified electrodes for DA determination

| Electrode material | Method | Detection Limit (μM) | Linear Range (μM) | Refs |
|---|---|---|---|---|
| Pd NP-rGO | LSV | 0.233 | 1-150 | 26 |
| Pd-NC-rGO | Amperometry | 7.02 | 20-220 | 27 |
| GNS-CNTs-$MoS_2$ | DPV | 0.05 | 0.1-100 | 28 |
| Au NP-PANI | Amperometry | 0.8 | 3-115 | 29 |
| (GQDs–$NHCH_2CH_2NH$) | DPV | 0.115 | 1.0-150 | 30 |
| Pt NP-rGO | Amperometry | 0.03 | 0.03-8.13 | 31 |
| N-doped rGO | DPV | 0.25 | 5-170 | 32 |
| Chitosan-GR | DPV | 1 | 1-24 | 33 |
| graphene | CV | 0.5 | 2.5-100 | 34 |
| 3D-f-$MoS_2$-rGO | DPV | 0.05 | 0.2-150 | This work |

*3.6 Selectivity, stability and reproducibility*

The selectivity of the signal response is vital to a sensor, especially for practical application as most of real samples are complex system with many potential interferences. As we all know, UA and AA always coexist with DA, thus the ability to selective detection or simultaneous detection of DA in

the presence of UA and AA is of great significance. Here, the presence of AA and UA on the oxidation current response of DA was investigated.

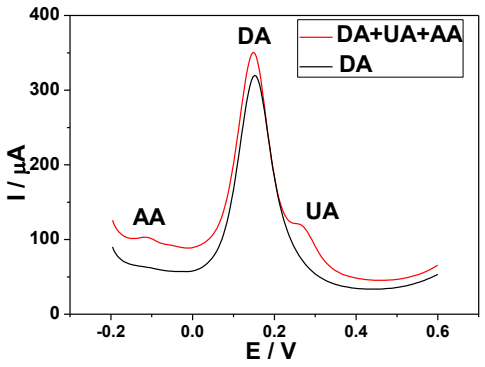


**Figure 7.** DPV curves of 1 mM DA in the absence of AA, UA (black curve) or in the presence of 4 mM AA and 4 mM UA obtained on 3D-f-$MoS_2$-rGO/GCE.

Fig. 7 shows the DPV curve of 1 mM DA with 4 mM AA and 4 mM UA obtained on 3D-f-$MoS_2$-rGO/GCE. The oxidation peak potentials appear at -0.114 V, 0.150 V and 0.265 V correspond to the oxidation of AA, DA and UA, respectively. Compared to the oxidation current of DA in the absence of co-existent molecules (curve b), the oxidation current of DA in the presence of AA and UA does not show obvious change, which indicates the presence of AA or UA does not interfere the detection of DA, revealing a good selectivity of 3D-f-$MoS_2$-rGO/GCE for dopamine detection. This selectivity may be ascribed to the different electrostatic interactions between electrode surface and molecules. Both AA (*pKa* = 4.1) and UA (*pKa* = 5.75) are negatively charged, while DA (*pKa* = 8.89) is positively charged in the pH 7.0 PBS. Therefore, DA is preferred to reach the negatively charged Nafion coated electrode to take part in electrochemical reaction due to the electrostatic attraction, while AA or UA is hard to reach the electrode surface due to the electrostatic repulsion. Although AA or UA is not totally repelled from the electrode, it is enough to achieve the accurate detection of DA without obvious interferences from AA or UA.

Besides sensitivity and selectivity, reproducibility and stability are another two important parameters for an electrochemical sensor. In this work, the fabrication reproducibility for five 3D-f-$MoS_2$-rGO/GCE was investigated by comparing their current responses to 1 mM DA. The calculated result shows that the relative standard deviation (RSD) of DA oxidation current is 3.62%, which is an acceptable reproducibility. The stability of the 3D-f-$MoS_2$-rGO/GCE was checked after it was stored in room temperature for one month. The current response only decreases 4.07% than the initial response, indicating a good stability.

### *3.7. Real sample analysis*

To verify the feasibility of the 3D-f-$MoS_2$-rGO/GCE in practical analysis, the fabricated sensor was used to detect DA in dopamine hydrochloride injection or in human serum samples using standard

addition method. All the samples were filtrated and diluted with PBS (pH 7.0) before the measurements.

**Table 2.** Determination and recovery test of DA in real samples (n = 3)

| Samples | Detected（μM） | Added (μM) | Found (μM) | Recovery (%) | RSD (%) |
|---|---|---|---|---|---|
| Injection solution | 25.36 | 10 | 34.78 | 98.4 | 1.52 |
| Human serum 1 | - | 10 | 9.78 | 97.8 | 1.37 |
| Human serum 2 | - | 20 | 19.73 | 98.7 | 1.42 |
| Human serum 3 | - | 30 | 30.88 | 102.9 | 2.18 |

As shown in Table 2, the recoveries of all measurements are in the range from 97.8% to 102.9%, which demonstrates satisfactory results in real samples determination.

## 4. CONCLUSIONS

In summary, a facile hydrothermal approach was employed to grow worm-like and flower-like $MoS_2$ on graphene sheet to form a 3D-f-$MoS_2$-rGO hybrid for sensitive electrochemical detection of dopamine. Introduction of graphene could enhance the conductivity of the hybrid and improve the dispersity of $MoS_2$, while the flower-like $MoS_2$ could reduce the aggregation of graphene sheet, and increase the active surface area. The synergistic interaction between rGO and $MoS_2$ endows the 3D-f-$MoS_2$-rGO hybrid a much better catalysis towards dopamine oxidation than single component rGO or $MoS_2$. Based on the hybrid, a non-enzymatic dopamine sensor with wide linear range, low detection limit, good selectivity and high stability was successfully prepared, which also shows promising application for real sample analysis.

ACKNOWLEDGEMENTS
This work is supported by the Natural Science Foundation of China (21665011), Science Foundation of Jiangxi Province (20161BAB203088), Scientific Research Funds of Jiangxi Normal University (No. 4506 and No. 4304).

## References

1. J.V. Lauritsen, J. Kibsgaard, S. Helveg, H. Topsoe, B.S. Clausen, E. Laegsgaard, F. Besenbacher, *Nat. Nanotechnol.*, 2 (2007) 53
2. Y. Huang, J. Guo, Y. Kang, Y. Ai, C.M. Li, *Nanoscale*, 7 (2015) 19358
3. H. Li, J.M.T. Wu, Z.Y. Yin, H. Zhang, *Acc. Chem. Res.*, 47 (2014) 1067
4. O. Lopez-Sanchez, D. Lembke, M. Kayci, A. Radenovic, A. Kis, *Nat. Nanotechnol.*, 8 (2013) 497
5. T.T. Shan, S. Xin, Y. You, H.P. Cong, S.H. Yu, A. Manthiram, *Angew. Chem. Int. Ed.*, 55 (2016)12783
6. X.R. Gan, H.M. Zhao, X. Quan, *Biosens. Bioelectron.*, 89 (2017) 56

7. S. Su, W.F. Cao, C. Zhang, X.Y. Han, H. Yu, D. Zhu, J. Chao, C.H. Fan, L.H. Wang, *RSC Adv.*, 6 (2016) 76614
8. Y. Shu, J.Y. Chen, Q. Xu, Z. Wei, F.P. Liu, R. Lu, S. Xu, X.Y. Hu, *J. Mater. Chem. B*, 5 (2017)1446
9. X.Y. Li, X.Z. Du, *Sens. Actuators B*, 239 (2017) 536
10. Y. Li, H.C. Lin, H. Peng, R.J. Qi, C.H. Luo, *Microchim. Acta*, 183(2016) 2517
11. H.L. Huang, W.H. Huang, Z.H. Yang, J.Y. Huang, J.D. Lin, W.P. Liu, Y.J. Liu, *J. Mater. Chem. A*, 5 (2017)1558
12. J. Peng, J. Weng, *Biosens. Bioelectron.*, 89 (2017) 652
13. F. Chekin, R. Boukherroub, S. Szunerits, *Mater. Sci. Eng. C*, 73 (2017) 627
14. F. Chekin, F. Teodorescu, Y. Coffinier, G.H. Pan, A. Barras, R. Boukherroub, S. Szunerits, *Biosens. Bioelectron.*, 85 (2016) 807
15. J.W. Zhou, J. Qin, N.Q. Zhao, C.S. Shi, E.Z. Liu, F. He, J.J. Lia, C.N. He, *J. Mater. Chem. A*, 4 (2016) 8734
16. Y.J. Zhai, J.H. Li, X.Y. Chu, M.Z. Xu, F.J. Jin, X. Li, X. Fang , Z.P. Wei, X.H. Wang, *J. Alloys and Compounds*, 672 (2016) 600
17. H.L. Shuai, K.J. Huang, Y.X. Chen, L.X. Fang, M.P. Jia, *Biosens. Bioelectron.*, 89 (2017) 989.
18. D.C. Marcano, D.V. Kosynkin, J.M. Berlin, A.S., Z.Z. Sun, A. Slesarev, L.B. Alemany, W. Lu, J.M. Tour, *ACS Nano*, 4 (2010) 4806
19. Y. Yan, X. Ge, Z. Liu, J.Y. Wang, J.M. Lee, X. Wang, *Nanoscale*, 5 (2013) 7768
20. H. Hwang, H. Kim, J. Cho, *Nano Lett.*, 11 (2011) 4826
21. X.-Y. Xu, Z.-Y. Yin, C.-X. Xu, J. Dai, J.-G. Hu, *Appl. Phy. Lett.*, 104 (2014) 033504
22. A. C. Ferrari, D.M. Basko, *Nat. Nanotechnol.*, 8 (2013) 235
23. A. Gupta, G. Chen, P. Joshi, S. Tadigadapa, P. C. Eklund, *Nano Lett.*, 6 (2006) 2667
24. H. Wang, X.J. Bo, L.P. Guo, *Sens. Actuators B*, 192 (2014) 181
25. G.R. Ma, M. Yang, C.Y. Li, H.Y. Tan, L. Deng, S. Xie, F.G. Xu, L. Wang, Y.H. Song, *Electrochim. Acta*, 220 (2016) 545
26. S. Palanisamy, S.H. Ku, S.M. Chen, *Microchim. Acta*, 180 (2013)1037
27. Y.S. Hsieh, B.D. Hong, C.L. Lee, *Microchim. Acta*, 183 (2016) 905
28. V. Mani, M. Govindasamy, S.M. Chen, R. Karthik, S. T. Huang, *Microchim. Acta*, 183 (2016) 2267
29. A.J. Wang, J.J. Feng, Y.F. Li, J.L. Xi, W.J. Dong, *Microchim. Acta*, 171 (2010) 431
30. Y.H. Li, Y.Y. Jiang, T. Mo, H.F. Zhou, Y.C. Lia, S.X. Li, J. Electroanal. Chem., 767 (2006) 84
31. C.L. Sun, H.H. Lee, J.M. Yang, C.C. Wu, *Biosens. Bioelectron.*, 26 (2011) 3450
32. Z.H. Sheng, X.Q. Zheng, J.Y. Xu, W.J. Bao, F.B. Wang, X.H. Xia, *Biosens. Bioelectron.*, 34 (2012)125
33. D.X. Han, T.T. Han, C.S. Shan, A. Ivaska, L. Niu, *Electroanalysis*, 22 (2010) 2001
34. X.Y. Ma, M.Y. Chao, Z.X. Wang, *Anal. Methods*, 4 (2012)1687